Xu et al. *Quantum Frontiers* (2022) 1:5
https://doi.org/10.1007/s44214-022-00005-x

Quantum Frontiers
上海交通大學 SHANGHAI JIAO TONG UNIVERSITY 李政道研究所 Tsung-Dao Lee Institute

ORIGINAL ARTICLE Open Access

Visualization of rotational symmetry breaking electronic states in $MnBi_2Te_4$ and $MnBi_4Te_7$

Hao-Ke Xu[1†], Fangsen Li[2†], Fu-Cong Fei[3†], Li Wang[2], Yi-Sheng Gu[1], Dang Liu[1], Qiao-Yan Yu[1], Sha-Sha Xue[1], Kun Peng[2], Bo Chen[3], Hang-Kai Xie[3], Zhen Zhu[1], Dan-Dan Guan[1], Shi-Yong Wang[1], Yaoyi Li[1], Canhua Liu[1], Fengqi Song[3], Hao Zheng[1*] and Jin-Feng Jia[1*]

Abstract

The Mn-Bi-Te class of compounds are recently discovered topological insulators with broken time-reversal-symmetry, which host unique quantum anomalous Hall and axion insulator states. Their key characteristics are believed to be sufficiently understood by models in a single-particle picture. Here, we apply scanning tunneling microscopy to study the electronic properties of $MnBi_2Te_4$ and $MnBi_4Te_7$. Unexpectedly, our quasiparticle interference (QPI) results demonstrate that rotational symmetry of the crystal breaks, *i.e.* a nematic-like pattern arises, in certain energy range but persists in others. Moreover, our data in the presence of an external magnetic field rule out the possibility of the material magnetism as an origin of the C_2 symmetric QPI pattern. This study reveals that the interaction in the Mn-Bi-Te class of topological materials may play an essential role in their electronic states, and thus opens a new path for investigating the interplay between wavefunction topology and symmetry breaking phases.

Keywords: Symmetry breaking, Nematic, Topological insulator, Scanning tunneling microscopy

1 Introduction

In a certain crystal, electron state with two-fold rotational (C_2) symmetry emerges despite its lattice obeys C_3 or C_4 symmetries. The electron state holding independent rotational symmetry, which differs from the symmetry of crystal structure, is named as rotational symmetry breaking phase. It is one of the important novel phenomena arising in many quantum materials, unconventional superconductors and strong correlated systems. Scientists have discovered many examples. Stripe order phase in cuprates is reported, where hidden-order phase is supposed to be the reason [1, 2]. Anisotropic transition driven by nematicity is found in iron arsenide [3–6], paving the way to find the true nature of charge order in this class of superconductors. Rotational symmetry breaking order in twisted graphene systems [7, 8] and nematic superconductivity in Bi_2Se_3 based topological superconductor candidates [9–11], make themselves good platforms for explaining strong correlation induced quantum phenomena. Those observations guarantee an important role that rotational symmetry breaking plays in quantum materials, for every discovery of rotational symmetry breaking phase in a condensed matter may open avenue toward new physics.

The Mn-Bi-Te class of materials are recently discovered topological insulators with inherent magnetic orderings that are predicted to host a variety of unusual phenomena [12–32]. Among them, the quantum anomalous Hall effect and axion insulator state probably have the highest significance and attract enormous research attentions.

*Correspondence: haozheng1@sjtu.edu.cn; jfjia@sjtu.edu.cn
[1]School of Physics and Astronomy, Key Laboratory of Artificial Structures and Quantum Control (Ministry of Education), Shenyang National Laboratory for Materials Science, Tsung-Dao Lee Institute, Shanghai Jiao Tong University, Shanghai 200240, China
Full list of author information is available at the end of the article †Equal contributors

Furthermore, many physicists believe the Mn-Bi-Te class of material is an ideal platform for magnetic topology research because the theoretical description is simple and sufficient. For example, theorists found that band theory together with strong spin-orbit coupling and Zeeman exchange field, *i.e.* a model within single-particle picture, is enough to capture the major physics of the material.

Scanning tunneling microscopy (STM) is a powerful technique to investigate topological materials [33–36], here we apply low temperature STM to examine the electronic states on ultra-high vacuum (UHV) cleaved $MnBi_2Te_4$ and $MnBi_4Te_7$ crystals. Surprisingly, our quasiparticle interference (QPI) patterns show a clearly violation of rotational symmetry of the crystal lattice, as well as a nematic-like electronic state at certain energies. We believe that understanding the facts necessitates a theory that goes beyond the single-particle picture.

2 Results and discussions

The simplest instance in the Mn-Bi-Te class of the magnetic topological insulators is $MnBi_2Te_4$. Its crystal is composed of layers of $MnBi_2Te_4$ that are stacked along the c axis (Fig. 1(a)). The spins in Mn atoms are believed to form ferromagnetic order in each $MnBi_2Te_4$ layer, and out-of-plane A-type antiferromagnetic (AFM) order between adjacent layers [12, 13]. Notably, the $MnBi_2Te_4$ crystal structure possess an out-of-plane C_3 rotational symmetry. It is also visible in our atomic resolution STM image (Fig. 1(b)). In the Fast Fourier Transforms (FFTs) of our STM images, we show that there are no distortion, reconstruction or specially shaped defects, which can break crystal's symmetry (Fig. S2, see Additional file 1). They are consistent with former findings [37–39]. Aside from the crystal lattice symmetry, electronic standing wave on the surface (Fig. 1(c)), which is resulted from the scattering of electronic state by local defects, establish QPI. QPI pattern collects the scattering vectors and display a C_6 rotational symmetry on our C_3 $MnBi_2Te_4$ crystal (Fig. 1(d)).

In order to gain insight of the electronic structure on the $MnBi_2Te_4$ surface, we take the dI/dV spectra (Fig. 1(e) and (f)). Based on the "V" shape of the dI/dV curve, we are able to find the energy of the surface Dirac point at −320 mV (according to the bottom of the "V"). Combining with our previous results [27], we can estimate the valence band maximum and conduction band minimum to be located at −450 mV and −220 mV respectively. In addition, we resolve a dip in dI/dV curve at the Fermi level. After we perform a line cut on QPI patterns and plot the scattering vector-energy diagram in Fig. 1(g), one can find that the QPI signal diminishes at the 0 mV, indicating that a gap opens at the Fermi level (since we can identify QPI signal at other adjacent energy, other origins that prevent existed states from scattering can be excluded). It represents an overlooked feature of the $MnBi_2Te_4$ crystal.

A more intriguing phenomenon occurs when we undertake a comprehensive QPI examination (Fig. 2). We observe "normal" QPI patterns with six-folds rotational symmetry in the energy from 200 meV to −50 mV, which lays in the bulk conduction band of $MnBi_2Te_4$. However, in the energy range of the surface state and the high energy part

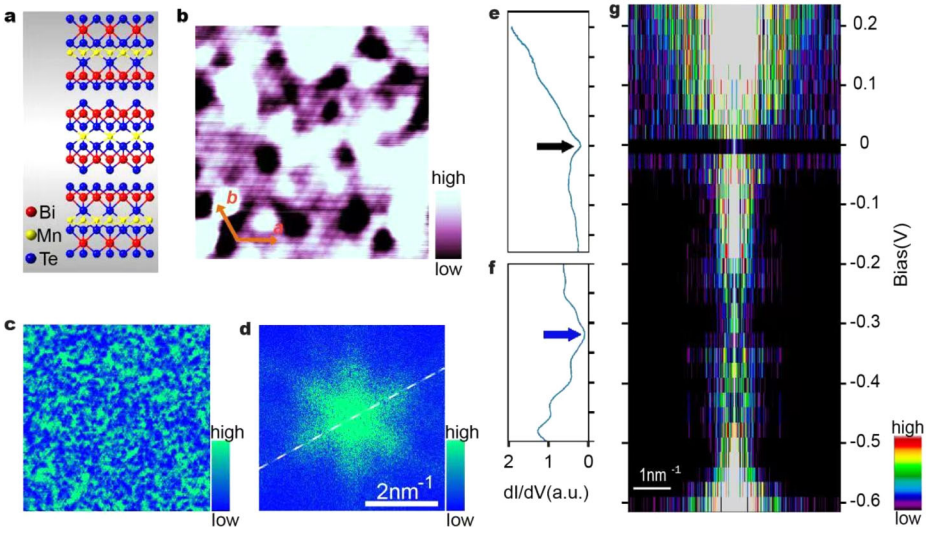

Figure 1 Surface electronic structure of $MnBi_2Te_4$. (**a**) Crystal structure of $MnBi_2Te_4$. (**b**) Typical topography of cleaved $MnBi_2Te_4$ surface with atomic resolution (10 nm × 10 nm). (**c**) LDOS maps on a flat $MnBi_2Te_4$ terrace (225 mV, 100 nm × 100 nm) (**d**) FFT of (**c**) which showing the QPI pattern of $MnBi_2Te_4$. (**e**) and (**f**) averaged dI/dV spectra measured on the same area, with energy range from 225 mV to −180 mV for e, and from −200 mV to −500 mV for f. Black arrow points to the gap at the Fermi level. Blue arrow indicates the position of surface Dirac node (−320 mV). (**g**) Energy-dependent QPI line-cut along Γ-M direction (indicated by the dashed line in panel (**d**))

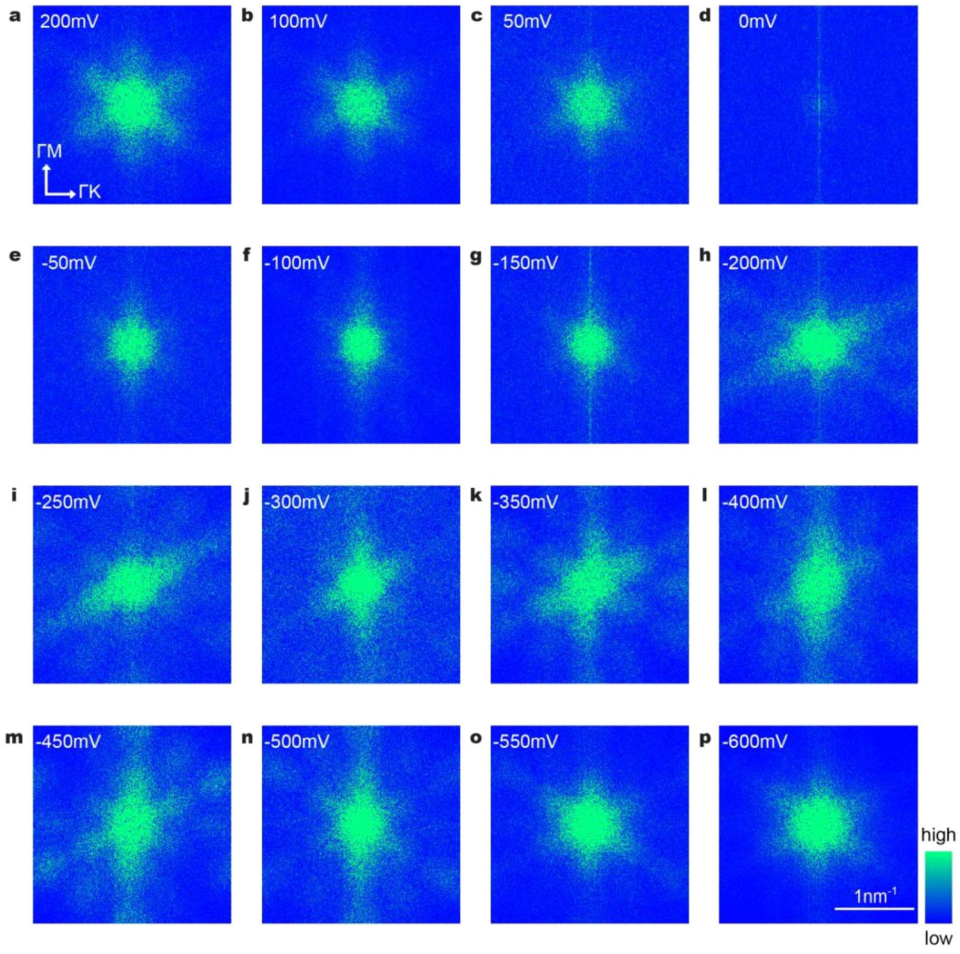

Figure 2 Rotational symmetry breaking QPIs of $MnBi_2Te_4$ surface. (**a**)-(**p**) a set of various energy layers of a dI/dV grid. (grid set point: –0.6 V 500 pA) clearly demonstrating the C_6 and C_2 symmetric QPI at different energies. For example, C_6 QPI patterns are shown in (**a**), (**b**) and (**p**), C_2 patterns can be remarkably observed in (**h**) to (**m**)

of valence band, our data unambiguously show that the QPI patterns take a nematic-like shape, obeying C_2 symmetry instead of C_6 (rotational symmetry of high energy QPI obeys). Since QPI patterns originate from the scatterings between electron states, we can conclude that the electron state breaks the C_3 rotational symmetry of the underline crystal. Interestingly, the C_6 symmetric QPI recovers when we approach the electronic state deeply in the valence band.

We also perform a systemic QPI study on its cousin material $MnBi_4Te_7$ as a control experiment. In contrast to the fact that $MnBi_2Te_4$ contains magnetic atoms in every layer, $MnBi_4Te_7$ has both magnetic $MnBi_2Te_4$ layers and non-magnetic Bi_2Te_3 layers in its bulk structure (Fig. 3(a)). Our dI/dV spectra on surfaces of both layers of $MnBi_4Te_7$ (Fig. S1) agree with previous findings [37, 38]. But unlike $MnBi_2Te_4$, we don't find any gaps at the Fermi levels of $MnBi_4Te_7$, which indicate the feature is not universal in the entire Mn-Bi-Te class. On the other hand, we do see a common unusual characteristic. Our QPI results show C_6 symmetric patterns on the magnetic layer surface of $MnBi_4Te_7$ in both higher positive and negative voltages, but a C_2 pattern at –400 mV (Fig. 3(b)-(e)). Notably, the QPI data in real space (Fig. 3(d)) display a distinct striped structure, which leads to the C_2 pattern in reciprocal space. Surprisingly, on the non-magnetic layer surface of $MnBi_4Te_7$, we also find the rotational symmetry breaking QPI in a particular energy range (Fig. 3(f)-(i)). Once more, the C_2 patterns are apparent in both real and reciprocal spaces (Fig. 3(h)). We combine the preceding results [40, 41] and our dI/dV spectra (Fig. S1) to determine the energies of bulk conduction and valence bands. We establish that the C_2 electronic structure in $MnBi_4Te_7$ also appears in the energy range where surface state and upper part of the bulk valence band are situated, after carefully reviewing the systematic voltage-dependent QPI data in Figs. S3 and S4. We

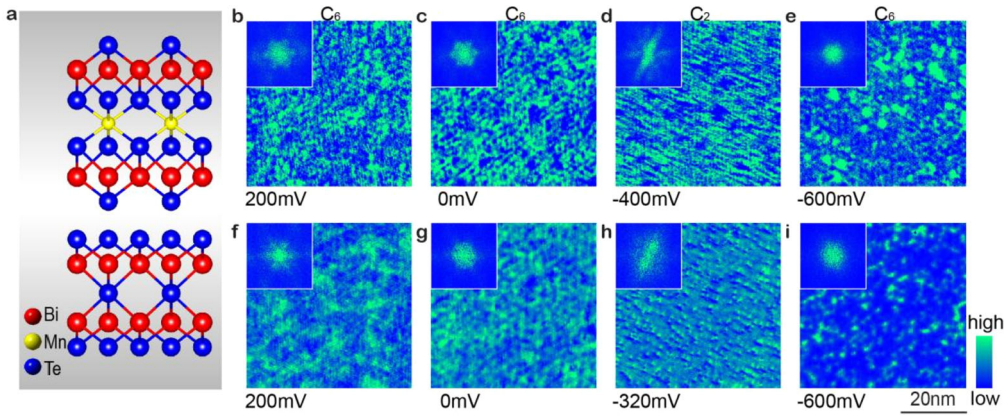

Figure 3 C_6 symmetry breaking QPIs on $MnBi_4Te_7$. (**a**) three-dimensional crystal structure of $MnBi_4Te_7$. Two different van de Waals layers can be distinguished, *i.e.* the upper layer containing Mn elements indicates $MnBi_2Te_4$ layer, the lower one without Mn atoms indicates Bi_2Te_3 layer. (**b**)-(**e**) LODS maps at indicated energies on $MnBi_2Te_4$ surface. Insets are the corresponding FFT. The C_2 QPI patterns are clearly revealed at –400 mV in both real and reciprocal spaces. (**f**)-(**i**) same as (**b**)-(**e**) but measured on Bi_2Te_3 surface, the C_6 symmetry breaking is discerned at energy of –320 mV

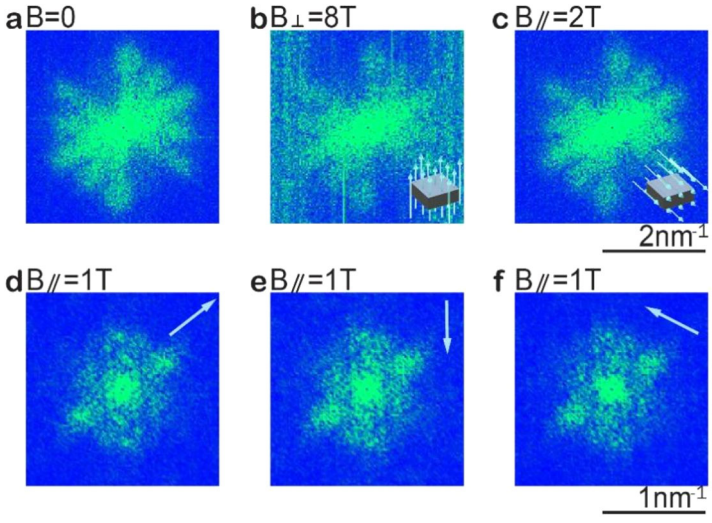

Figure 4 QPI patterns under applied magnetic field. (**a**) QPI on a $MnBi_2Te_4$ sample at –240 mV, displaying C_2 rather than C_6 symmetry. (**b**) and (**c**) same as a but under an 8T out of plane and 2T in plane magnetic field, respectively. (**d**)-(**f**) QPI patterns on the Bi_2Te_3 termination of a $MnBi_4Te_7$ sample (–0.3 V 500 pA). 1T in plane magnetic fields are applied along three Γ-M directions. The directions of the C_2 patterns do not change with magnetic fields

emphasis that our $MnBi_2Te_4$ and $MnBi_4Te_7$ samples were measured by two different STM apparatuses (see method section). It thus rules out the instrumental artificial effect as an interpretation of the C_2 symmetry QPIs.

Moreover, we carry out magnetic field dependent experiments. During the QPI measurement on $MnBi_2Te_4$, we have applied either 8T out-of-plane field or 2T in-plane field to the sample but find no noticeable difference in the C_2 symmetric patterns (Fig. 4(a)-(c)). Previous result suggests that magnetic field of up to 7T is capable of aligning all spins out-of-plane [27], thus our field is strong enough to eradicate the possibility that the spin alignment may take part in breaking C_3 symmetry. However, our QPI data still takes a nematic-like shape in the presence of B_z = 8T. Furthermore, we take the QPI measurements on the non-magnetic layer of $MnBi_4Te_7$ with applying in-plane fields along three Γ-M directions (Fig. 4(d)-(f)). The three cases show almost same C_2 QPI images. If the QPI's C_2 relate to magnetic field (magnetic field can align all spin in plane, which can also induce C_2 symmetry), the C_2 axis should rotate along with magnetic field direction, since it doesn't

rotate, we thus believe that C_2 symmetry is not caused by magnetic structure.

Despite the fact that the Mn-Bi-Te class of materials has been viewed as a simple and ideal magnetic topological insulator, unexpected observations continue to emerge. A notable example is the experimental detected gapless Dirac cones on $MnBi_2Te_4$ and $MnBi_4Te_7$ surfaces, which should be gapped due to the time reversal symmetry breaking in these compounds. This issue deserves interests of the researchers. Indeed, theorists start using band theories together with various attempted magnetic configurations to solve the problem [16, 25, 28–31]. Some researchers speculate that whereas $MnBi_2Te_4$ and $MnBi_4Te_7$ bulks exhibit out-of-plane A-type AFM, the magnetic ordering on their surfaces may differ from the ideal case, *i.e.* the surface magnetization has an in-plane component [16, 37]. Up to our knowledge, we are not aware of any report that predicts or detects similar rotational symmetry breaking electronic state in the Mn-Bi-Te class of magnetic topological insulators. Following the logic of previous argument on the gap issue, it is natural to speculate that the suggested complex magnetism is the plausible driver of the C_2 symmetric QPIs. However, the magnetism-driven electronic nematicity exhibits a reaction to an external applied field [42], which is contrast to our field dependent experimental results. It is also possible that the magnetic field fail to control nematic states, which is mainly because that the state energy is far from Fermi level. Within the experimental evidence, it is difficult to relate our C_2 state to the magnetism of $MnBi_2Te_4$ and $MnBi_4Te_7$ samples. The physics of $MnBi_2Te_4$ family is still far from being understood even when we consider magnetic interaction. As a result, a theory that takes into account various interactions in these crystals is required.

Next, we want to discuss the nature of nematic-like states although they emerge in the energy range which includes a part below bulk VBMs of $MnBi_2Te_4$ and $MnBi_4Te_7$. According to the single-particle band simulation, we know that the surface state does not immediately merge into the valence band at the energy below the bulk VBM [13–16]. They stay away from each other in a large energy range. On the other hand, QPI will be dominated by surface standing wave even when surface state and bulk state coexist. It becomes possible that our uncovered C_2 state mainly comes from the surface state. Therefore, it is reasonable to expect that a thorough solution of C_2 electronic state can also provide a hitherto missed hint to the surface Dirac gap issue in $MnBi_2Te_4$ and $MnBi_4Te_7$.

As a summary, we discover a rotational symmetry breaking state in the magnetic topological insulators $MnBi_2Te_4$ and $MnBi_4Te_7$. C_2 symmetric QPI patterns are clearly resolved at the energy range where surface state and high energy part of the bulk valence band are located. We find that these electronic states are resistant to external magnetic fields, proving that they are generated by a non-magnetic mechanism. Our findings suggest that the interaction and interplay in spin, orbit, charge and lattice degrees of freedom may play a substantial role in the magnetic topological insulators $MnBi_2Te_4$ and $MnBi_4Te_7$. Exotic emergent phenomena and innovative quantum devices are made conceivable by the coexistence of topological band and symmetry breaking order in a same sample.

3 Methods

The single crystalline samples of $MnBi_2Te_4$ and $MnBi_4Te_7$ are grown by flux-assisted method. The reactants MnTe and Bi_2Te_3 are mixed in the molar ratio MnTe: Bi_2Te_3 = 1:5.8 and 1:7.0 for $MnBi_2Te_4$ and $MnBi_4Te_7$ respectively, are placed into an alumina crucible and sealed by a quartz tube. We then put the sealed quartz tube into a muffle furnace and heat them up to 950°C in 24 hours. We keep this temperature for 12 hours to ensure that the materials melt homogenic. Finally, the sealed quartz tube was slowly cooled down to 578°C and 575°C for $MnBi_2Te_4$ and $MnBi_4Te_7$ respectively in 24 hours. We take the quartz tubes out from the muffle furnace rapidly and decant them with centrifuge to separate the shining plate-like crystals from the excess Bi_2Te_3 flux.

$MnBi_2Te_4$ samples are measured by a commercial STM (Unisoku 1300) in Suzhou Institute of Nano-Tech and Nano-Bionics. Our samples are cleaved in UHV circumstance (better than 2×10^{-10} Torr) at 80K. After cleaving, the sample is transferred to measurement stage within 20 mins, and then cooled down to 4.5K. All measurements are conducted at 4.5K, in UHV. Chemical etched Pt/Ir wire is used as STM tip, which is prepared by electron beam heating. Lock-in amplifier is applied to detect dI/dV signals, with modulation of 5 mV and 991 Hz. $MnBi_4Te_7$ samples are measured by Unisoku 1600 STM in Shanghai Jiao Tong university. The samples are cleaved in UHV (better than 1×10^{-9} Torr), but at room temperature. After being transferred to STM head, the samples are cooled down to 4.5K in 25 mins for STM measurements. The STM tips are etched tungsten wire followed by electron beam annealing. dI/dV data are acquired with lock-in amplifier with 5 mV and 991 Hz modulation.

Supplementary information

Supplementary information accompanies this paper at https://doi.org/10.1007/s44214-022-00005-x.

Additional file 1. Supplementary information (DOCX 868 kB)

Acknowledgements
We thank Q.-H. Liu and Y. Xu for the helpful discussions.

Funding
We thank the NSFC (Grants No. 11790313, No. 92065201, No. 11874256, No. 11874258, No. 12074247, No. 12174252, No. 11861161003, No. 12025404, No. 11904165, No. 92161201, No.12104221, and No. 12074181), Ministry of Science and Technology of China (Grants No. 2019YFA0308600, 2020YFA0309000,2017YFA0303203), the Strategic Priority Research Program of Chinese Academy of Sciences (Grant No. XDB28000000) and the Science and Technology Commission of Shanghai Municipality (Grants No. 2019SHZDZX01, No. 19JC1412701, No. 20QA1405100), F.-Q. Song thanks the Natural Science Foundation of Jiangsu Province (Grant Nos. BK20200312, BK20200310, and BK20190286) or partial support. F. S. Li also acknowledge financial support from the Suzhou Science and Technology Program (Grant No. SJC2021009) and the Youth Innovation Promotion Association of Chinese Academy of Sciences (2017370).

Availability of data and materials
All data generated or analyzed during this study are included in this article and its supplementary information files.

Declarations

Competing interests
Jin-feng Jia is the Executive Editor for Quantum Frontiers and was not involved in the editorial review, or the decision to publish, this article. All authors declare that there are no competing interests.

Author contribution
HX did the STM experiments with the help of FL, LW, YG, DL, QY, SX, KP, ZZ, DG, SW, YL and CL. FF, BC, HX, and FS grow the materials. HZ and JJ supervise the project. All authors read and approved the final manuscript.

Author details
[1]School of Physics and Astronomy, Key Laboratory of Artificial Structures and Quantum Control (Ministry of Education), Shenyang National Laboratory for Materials Science, Tsung-Dao Lee Institute, Shanghai Jiao Tong University, Shanghai 200240, China. [2]Vacuum Interconnected Nanotech Workstation, Suzhou Institute of Nano-Tech and Nano-Bionics, Chinese Academy of Sciences, Suzhou 215123, China. [3]National Laboratory of Solid State Microstructures, Collaborative Innovation Center of Advanced Microstructures, and College of Physics, Nanjing University, Nanjing 210093, China.

Publisher's Note
Springer Nature remains neutral with regard to jurisdictional claims in published maps and institutional affiliations.

Received: 27 April 2022 Revised: 18 July 2022 Accepted: 20 July 2022
Published online: 23 September 2022

References
1. Kivelson SA, Fradkin E, Emery VJ (1998) Electronic liquid-crystal phases of a doped Mott insulator. Nature 393:550–553
2. Zhao H, Ren Z, Rachmilowitz B et al (2019) Charge-stripe crystal phase in an insulating cuprate. Nat Mater 18:103–107
3. Chu JH, Analytis JG, Greve KD, McMahon PL, Islam Z, Yamamoto Y, Fisher IR (2010) In-plane resistivity anisotropy in an underdoped iron arsenide superconductor. Science 329:824–826
4. Chuang TM, Allan MP, Lee JH, Xie Y, Ni N, Bud'ko SL, Boebinger GS, Canfield PC, Davis JC (2010) Nematic electronic structure in the "parent" state of the iron-based superconductor $Ca(Fe_{1-X}Co_x)_2As_2$. Science 327:181–184
5. Rosenthal EP, Andrade EF, Arguello CJ, Fernandes RM, Xing LY, Wang XC, Jin CQ, Millis AJ, Pasupathy AN (2014) Visualization of electron nematicity and unidirectional antiferroic fluctuations at high temperatures in NaFeAs. Nat Phys 10:225–232
6. Li W, Zhang Y, Deng P, Xu ZL, Mo S-K, Yi M, Ding H, Hashimoto M, Moore RG, Lu D-H, Chen X, Shen Z-X, Xue QK (2017) Stripes developed at the strong limit of nematicity in FeSe film. Nat Phys 13:957–961
7. Jiang Y et al (2019) Charge order and broken rotational symmetry in magic-angle twisted bilayer graphene. Nature 573:91–95
8. Rubio-Verdú C, Turkel S, Song Y et al (2021) Moiré nematic phase in twisted double bilayer graphene. Nat Phys online
9. Yonezawa S, Tajiri K, Nakata S et al (2017) Thermodynamic evidence for nematic superconductivity in $Cu_xBi_2Se_3$. Nat Phys 13:123–126
10. Asaba T, Lawson BJ, Tinsman C, Chen L, Corbae P, Li G, Qiu Y, Hor YS, Fu L, Li L (2017) Rotational symmetry breaking in a trigonal superconductor Nb-doped Bi_2Se_3. Phys Rev X 7:011009
11. Tao R, Yan YJ, Liu X, Wang ZW, Ando Y, Wang QH, Zhang T, Feng DL (2018) Direct visualization of the nematic superconductivity in $Cu_xBi_2Se_3$. Phys Rev X 8:041024
12. Tao R, Yan YJ, Liu X, Wang ZW, Ando YC, Wang QH, Zhang T, Feng DL (2018) Direct visualization of the nematic superconductivity in $Cu_xBi_2Se_3$. Phys Rev X 8:041024
13. Li JH, Li Y, Du SQ, Wang Z, Gu BL, Zhang SC, He K, Duan WH, Xu Y (2019) Intrinsic magnetic topological insulators in van der Waals layered $MnBi_2Te_4$-family materials. Sci Adv 5:eaaw5685
14. Otrokov MM, Klimovskikh II, Bentmann H, Estyunin D, Zeugner A, Aliev ZS, Gaß S, Wolter AUB, Vyazovskaya AY, Chulkov EV (2019) Prediction and observation of an antiferromagnetic topological insulator. Nature 576:416–422
15. Chen YJ, Xu LX, Li JH, Li YW, Wang HY, Zhang CF, Li H, Wu Y, Liang AJ, Chen C, Jung SW, Cacho C, Mao YH, Liu S, Wang MX, Guo YF, Xu Y, Liu ZK, Yang LX, Chen YL (2019) Topological electronic structure and its temperature evolution in antiferromagnetic topological insulator $MnBi_2Te_4$. Phys Rev X 9:041040
16. Hao YJ, Liu PF, Feng Y, Ma XM, Schwier EF, Arita M, Kumar S, Hu CW, Lu R, Zeng M, Wang Y, Hao ZY, Sun HY, Zhang K, Mei JW, Ni N, Wu LS, Shimada K, Chen CY, Liu QH, Liu C (2019) Gapless surface Dirac cone in antiferromagnetic topological insulator $MnBi_2Te_4$. Phys Rev X 9:041038
17. Li H et al (2019) Dirac surface states in intrinsic magnetic topological insulators $EuSn_2As_2$ and $MnBi_2nTe_{3n+1}$. Phys Rev X 9:041039
18. Liu C, Wang YC, Li H, Wu Y, Li YX, Li JH, He K, Xu Y, Zhang JS, Wang YY (2020) Robust axion insulator and Chern insulator phases in a two-dimensional antiferromagnetic topological insulator. Nat Mater 19:522
19. Deng YJ, Yu YJ, Shi MZ, Guo ZG, Xu ZH, Wang J, Chen XH, Zhang YB (2020) Quantum anomalous Hall effect in intrinsic magnetic topological insulator $MnBi_2Te_4$. Science 367:895
20. Ge J, Liu YZ, Li JH, Li H, Luo TC, Wu Y, Xu Y, Wang J (2020) High-Chern-number and high temperature quantum Hall effect without Laudau levels. Natl Sci Rev 7:1280
21. Zhao YF, Zhou LJ, Wang F, Wang G, Song TC, Ovchinnikov D, Yi HM, Mei R et al (2021) Even–odd layer-dependent anomalous Hall effect in topological magnet $MnBi_2Te_4$ thin films. Nano Lett 21:7691–7698
22. Swatek P, Wu Y, Wang LL, Lee K, Schrunk B, Yan J, Kaminski A (2020) Gapless Dirac surface in the antiferromagnetic topological insulator $MnBi_2Te_4$. Phys Rev B 101:161109
23. Ma XM, Chen ZJ, Schwier DF, Zhang Y, Hao YJ, Kumar S, Lu R, Shao JF et al (2020) Hybridization-induced gapped and gapless states on the surface of magnetic topological insulators. Phys Rev B 102:245136
24. Lee SH, Zhu YL, Wang Y, Miao LX, Pillsbury T, Yi H, Kempinger S et al (2019) Spin scattering and noncollinear spin structure-induced intrinsic anomalous Hall effect in antiferromagnetic topological insulator $MnBi_2Te_4$. Phys Rev Res 1:012011
25. Hu Y, Xu LX, Shi MZ, Luo ZY, Peng ST, Wang ZY, Ying JJ, Wu T, Liu ZK, Zhang CF, Chen YL, Xu G, Chen XH, He JF (2020) Universal gapless Dirac cone and tunable topological states in $(MnBi_2Te_4)m(Bi_2Te_3)_n$ heterostructures. Phys Rev B 101:161113
26. Klimovskikh II, Otrokov MM, Estyunin D et al (2020) Tunable 3D/2D magnetism in the $(MnBi_2Te_4)$ $(Bi_2Te_3)_m$ topological insulators family. npj Quantum Mater 5:54
27. Chen B, Fei F, Zhang D et al (2019) Intrinsic magnetic topological insulator phases in the Sb doped $MnBi_2Te_4$ bulks and thin flakes. Nat Commun 10:4469
28. Sun H-P et al (2020) Analytical solution for the surface states of the antiferromagnetic topological insulator $MnBi_2Te_4$. Phys Rev B 102:241406(R)
29. Garrity KF, Chowdhury S, Tavazza FM (2021) Topological surface states of $MnBi_2Te_4$ at finite temperatures and at domain walls. Phys Rev Mater 5:024207
30. Chen WZ, Zhao YF, Yao QS, Zhang J, Liu QH (2021) Koopmans' theorem as the mechanism of nearly gapless surface states in self-doped magnetic topological insulators. Phys Rev B 103:L201102
31. Shikin AM, Estyunin DA, Zaitsev NL, Glazkova D, Klimovskikh II, Filnov SO, Rybkin AG et al (2021) Sample-dependent Dirac-point gap in $MnBi_2Te_4$

and its response to applied surface charge: a combined photoemission and ab initio study. Phys Rev B 104:115168
32. Xu HK, Gu MQ, Fei FC, Gu YS, Liu D, Yu QY, Xue SS, Ning XH, Chen B, Xie HK, Zhu Z, Guan DD, Wang SY, Li YY, Liu CH, Liu QH, Song FQ, Zheng H, Jia JF (2022) Observation of magnetism-induced topological edge state in antiferromagnetic topological insulator $MnBi_4Te_7$. ACS Nano 16:9810–9818
33. Zheng H, Xu SY, Bian G, Guo C, Chang GQ, Sanchez DS, Belopolski I, Lee CC, Huang SM, Zhang X et al (2016) Atomic-scale visualization of quantum interference on a Weyl semimetal surface by scanning tunneling microscopy. ACS Nano 10:1378–1385
34. Zhu Z, Chang TR, Huang CY, Pan HY, Nie XA, Wang XZ, Jin ZT, Xu SY, Huang SM, Guan DD, Wang SY, Li YY, Liu CH, Qian D, Ku W, Song FQ, Lin H, Zheng H, Jia JF (2018) Quasiparticle interference and nonsymmorphic effect on a floating band surface state of ZrSiSe. Nat Commun 9:4153
35. Nie XA, Li SJ, Yang M, Zhu Z, Xu HK, Yang X, Zheng FW, Guan DD, Wang SY, Li YY, Liu CH, Li J, Zhang P, Shi YG, Zheng H, Jia JF (2020) Robust hot electron and multiple topological insulator states in $PtBi_2$. ACS Nano 14:2366–2372
36. Zhu Z, Papaj M, Nie XA, Xu HK, Gu YS, Yang X, Guan DD, Wang SY, Li YY, Liu CH, Luo JL, Xu ZA, Zheng H, Fu L, Jia JF (2021) Discovery of segmented Fermi surface induced by cooper pair momentum. Science 374:1381–1385
37. Yuan YH, Wang XT, Li H, Li JH, Ji Y, Hao ZQ, Wu Y, He K, Wang YY, Xu Y, Duan WH, Li W, Xue QK (2020) Electronic states and magnetic response of $MnBi_2Te_4$ by scanning tunneling microscopy and spectroscopy. Nano Lett 20:3271
38. Liang ZW, Luo AY, Shi MZ, Zhang Q, Nie SM, Ying JJ, He JF, Wu T, Wang ZJ, Xu G, Wang ZY, Chen XH (2020) Mapping Dirac fermions in the intrinsic antiferromagnetic topological insulators $(MnBi_2Te_4)(Bi_2Te_3)_n$ (n = 0, 1). Phys Rev B 102:161115
39. Wu XF, Li JY, Ma XM, Zhang Y, Liu YT, Zhou CS, Shao JF, Wang QM, Hao YJ, Feng Y et al (2020) Distinct topological surface states on the two terminations of $MnBi_4Te_7$. Phys Rev X 10:031013
40. Chen B, Wang DH, Jiang ZC, Zhang B, Cui ST, Guo JW, Xie HK et al (2021) Coexistence of ferromagnetism and topology by charge carrier engineering in the intrinsic magnetic topological insulator $MnBi_4Te_7$. Phys Rev B 104:075134
41. Li JH, Wang C, Zhang ZT, Gu BL, Duan WH, Xu Y (2019) Magnetically controllable topological quantum phase transitions in the antiferromagnetic topological insulator $MnBi_2Te_4$. Phys Rev B 100:121103
42. Yin JX, Zhang SS, Li H et al (2018) Giant and anisotropic many-body spin–orbit tunability in a strongly correlated kagome magnet. Nature 562:91–95